IMPACTS OF SOLAR STORM EVENTS AND ION BEAM EMISSION ON ELECTROSTATIC TRACTOR PERFORMANCE

Erik A. Hogan and Hanspeter Schaub

13th Spacecraft Charging Technology Conference

Pasadena, California **June 23–27, 2014**

Impacts of Solar Storm Events and Ion Beam Emission on Electrostatic Tractor Performance

Erik A. Hogan and Hanspeter Schaub

***Abstract*—A recent proposed technique for GEO debris mitigation is the electrostatic tractor. The tug vehicle approaches a debris object within 5-10 craft radii and emits a focused electron beam onto it. This results in a negative charge on the debris, and a positive charge on the tug vehicle. Used in conjunction with low thrust, the electrostatic force is used to tow a debris object into a disposal orbit. In this study, the impacts of geomagnetic storm activity on the charging of tug and debris are considered. The influence of electrons emitted from the deputy (photo- and secondary electrons) on tug charging are also considered. Both of these phenomena yield improved electrostatic tractor performance. The simultaneous emission of an electron and ion beam by the tug is also considered to improve tractor performance and enable charge transfer for scenarios where it fails when only an electron beam is used. The theoretical maximum electrostatic force that is possible with simultaneous emission is computed, and the results indicate that emitting both an electron and ion beam enables smaller tug vehicles to tow larger objects that could not otherwise be towed with only an electron beam.**

***Index Terms*—Electrostatic tractor, spacecraft charge control, geomagnetic storm impacts on charging**

I. Introduction

The high value of the geostationary ring (GEO), coupled with the increasing number of orbital debris, highlights the need for active debris removal methods.[1], [2], [3] When spacecraft reach end-of-life in GEO, international guidelines call for reorbiting into a disposal orbit typically 200-300 km above GEO.[4], [5] For debris objects that do not possess the ability for reorbiting, an external method is needed to reach the disposal orbit. Originally proposed as a means for asteroid deflection,[6] the electrostatic tractor has been suggested as a means for GEO debris remediation.[7] The concept relies on a combination of an attractive electrostatic force between two craft and low thrusting capability on one of the craft, as illustrated in Figure 1. The attractive force acts as a virtual tether between the two objects, and a low thrust maneuver is used to tow the noncooperative, possibly tumbling large debris object into a new orbit.[8] GEO debris can be tumbling up to 10's of degrees per second,[9] making any physical docking methods particularly challenging.[10] The electrostatic tractor method allows the tumbling object to be reorbited without first having to despin it. Considering non-symmetrical spacecraft geometries, the charging also gives rise to torques on the craft.[11], [12], [13] Through careful manipulation of the charging histories, these torques can be applied in a manner sufficient to despin a noncooperative object remotely.[12] This latter ability greatly simplifies any orbital servicing mission where great efforts are required to first despin objects spinning at 1 degree per second or greater.[14], [10]

E. A. Hogan and H. Schaub are with the Colorado Center for Astrodynamics Research, University of Colorado, Boulder, CO 80309-0431, USA (e-mail: erik.hogan@colorado.edu, hanspeter.schaub@colorado.edu)

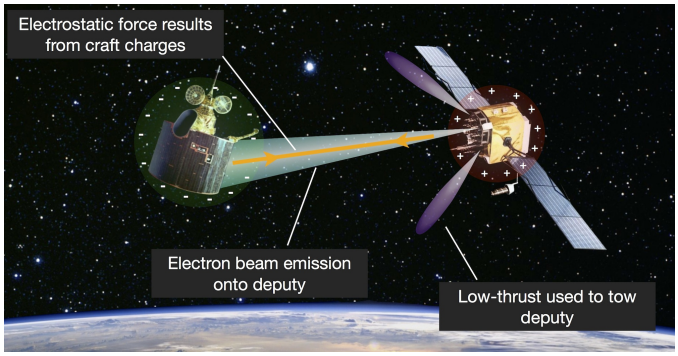

Fig. 1. Illustration of electrostatic tractor concept.

For the electrostatic tractor application, a method of active charge control is needed. Charged particle beams are the most ideal candidates for this purpose. Emitting a high-energy beam (10s of keV) at sufficient current levels enables the tug to reach high potentials. Either an ion or electron beam may be used, though an electron beam is preferred due to its simpler implementation and reduced momentum transfer.[12] Directing the beam onto the deputy provides a current that will affect the deputy charging, much like the natural charging that occurs due to the plasma environment. The vast majority of prior work with Coulomb formations merely assume either a charge or a potential on the different spacecraft in the formation, without actually modeling the mechanism for and environmental influences on achieving the charging.[15], [16], [17], [18], [12], [8], [19], [20] The electrostatic tractor performance is dependent on the charging that is achieved with electron or ion beam emission, and it is important to characterize the charge transfer process. Reference [12] presents a first-order charging model to compute potentials on tug and deputy as a function of various environmental current sources, applied to the electrostatic tractor problem. Assuming an electron beam is used for charge control, one particular tug and deputy configuration is considered, and the resulting electrostatic forces are computed for specific space weather conditions. The work does not consider the impact of solar storm events on tractor performance, or the simultaneous use of electron and ion beam emission for improved performance. This first-order charging model provides the tools needed to

analyze the general charging trends that may be encountered for the electrostatic tractor application, and is used extensively in the current study.

The charging of a spacecraft is dependent on the space plasma environment.[21], [22] Because of the potential threats to mission viability caused by charging events, much work has been done to characterize the space weather environment both in LEO and GEO.[23], [24] The plasma environment is typically characterized by two parameters: density and temperature. The LEO plasma environment is much colder and denser than in GEO, with typical LEO densities ranging from $10^4 - 10^6$ particles/cm^{-3} and corresponding temperatures below 1 eV. In GEO, the plasma densities are orders of magnitude smaller, ranging from $.1 - 10$ particles/cm^{-3}. Depending on geomagnetic storm activity, ion temperatures may range from below 100 eV to 20 keV or more. Electron temperatures are typically above 1 keV, and may reach tens of keV depending on storm activity.

The severity of geomagnetic storms is classified using the k_p index, which is based on the observed variation in the degree of irregular magnetic activity throughout each day, observed at various ground stations.[25] The k_p index utilizes an integer scale ranging from 0-9, and values of 5 and up indicate that a geomagnetic storm is occurring. The National Oceanic and Atmospheric Administration (NOAA) has also developed a scale for classifying the severity of geomagnetic storms.[26] The scale ranges from G-1 minor storms ($k_p = 5$) to G-5 extreme storms ($k_p = 9$). The NOAA scale provides information about expected impacts to spacecraft for different storm levels. In a minor storm (G-1, $k_p = 5$), minimal impacts to spacecraft operations can be expected. At the other end of the spectrum, an extreme storm (G-5, $k_p = 9$) may cause extensive surface charging, loss of attitude, and problems with communications and satellite tracking. Fortunately, stronger storms only occur a few times per eleven year solar cycle. The frequency of occurrence for the various storm conditions in a typical solar cycle is shown in Figure 2. The vast majority of the time ($> 85\%$), there is either no storm activity or a minor storm occurrence.

In prior work considering environmental impacts on electrostatic tractor performance, quiet storm conditions are used.[27] Further, only electron beam emission is considered as a means for charge control.[12], [27] Reference [28] illustrates that when the deputy sizes are roughly the same as or larger than the tug, it becomes very difficult for charge transfer to occur when only an electron beam is used. In the current study, several novel results are presented. First, the impacts of geomagnetic storm events on the charge transfer process are considered. These storm events lead to changes in the plasma environment in GEO, and change the charging behavior of the tug and deputy. To mitigate some of the relative sizing issues, simultaneous emission of an electron beam (onto the deputy) and an ion beam (into space) is considered as a means to improve charge transfer performance by providing an additional control variable for charge control. During charging, electrons are emitted from the deputy surface. In the vicinity

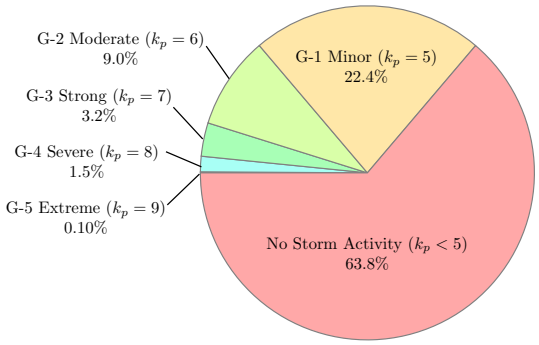

Fig. 2. Percent of days in an 11 year solar cycle for which various geomagnetic storm levels occur. Data adapted from [26].

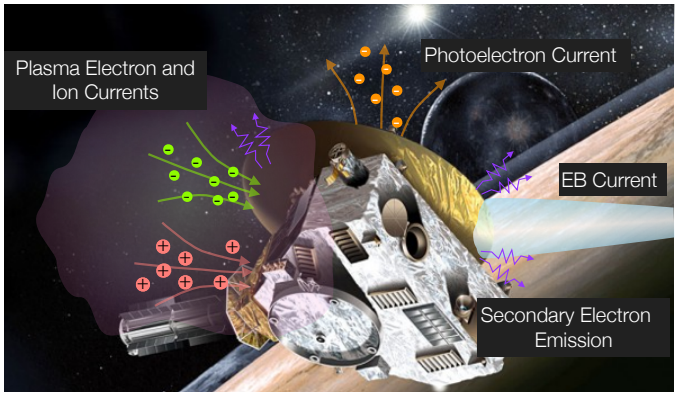

Fig. 3. Illustration of various current sources that affect spacecraft charging.

of the positively charged tug, some of these electrons will be recaptured. This back-flux has thus far not been investigated. In the current study, the impacts of this electron back-flux onto the tug on tractor performance are investigated, as well.

The paper is structured as follows. First, an overview of the charging and electrostatic force models is presented. Next, the influence of geomagnetic storm conditions on charging is presented and compared with quiet storm conditions. Then, the effects of the electron back-flux from deputy to tug on tractor performance are investigated. Lastly, the simultaneous emission of an electron and ion beam is considered, and the performance benefits that result are characterized.

II. Background

A. Charge Transfer Model

The electrostatic tugging force used for towing is dependent on the charging that occurs on both the tug and deputy. Several factors influence this charging process. Naturally occurring ion and electron plasma currents are collected by the spacecraft, and photoelectrons may be emitted depending on the spacecraft potential and presence of sunlight. Focused electron beam emission by the tug is used for charge control. When the electron beam is absorbed by the deputy, secondary electron emission occurs as the incoming beam electrons excite and release electrons from the deputy surface material. The potential levels achieved by the tug and deputy result from

a balance of these various current sources, which are illustrated in Figure 3. To compute these potentials, the charging model developed in [29] is applied.

A photoelectron current occurs whenever the spacecraft are in sunlight. This current is modeled by[21]

$$I_{ph}(\phi) = j_{ph,0} A_\perp e^{-\phi/T_{ph}} \qquad \phi > 0 \qquad (1a)$$
$$= j_{ph,0} A_\perp \qquad \phi \leq 0 \qquad (1b)$$

where ϕ is the spacecraft potential, $T_{ph} = 2$ eV is the temperature of the emitted photoelectrons, $j_{ph,0} = 20\ \mu\text{A/m}^2$ is the photoelectron flux, and $A_\perp$ is the cross-sectional area exposed to sunlight. For the spherical geometries assumed here, $A_\perp = \pi r^2$. For high positive potentials, the photoelectron current is effectively zero because all of the emitted electrons are recaptured.

The plasma electron current is modeled by[30]

$$I_e(\phi) = -\frac{Aqn_e w_e}{4} e^{\phi/T_e} \qquad \phi < 0 \qquad (2a)$$
$$= -\frac{Aqn_e w_e}{4}\left(1 + \frac{\phi}{T_e}\right) \qquad \phi \geq 0, \qquad (2b)$$

where A is the surface area exposed to the plasma environment, T_e is the plasma electron temperature, n_e is the plasma electron density, q is the elementary charge, and $w_e = \sqrt{8T_e/\pi m_e}$ is the thermal velocity of the electrons. The electron mass is represented by m_e. Note that for large negative potentials, I_e is very small. This is due to the fact that electrons are repelled by the negatively charged spacecraft. Similarly, the plasma ion current is computed using[30]

$$I_i(\phi) = \frac{Aqn_i w_i}{4} e^{-\phi/T_i} \qquad \phi > 0 \qquad (3a)$$
$$= \frac{Aqn_i w_i}{4}\left(1 - \frac{\phi}{T_i}\right) \qquad \phi \leq 0, \qquad (3b)$$

where $w_i = \sqrt{8T_i/\pi m_i}$. Note that the variable quantities represent the same parameters as before, except the subscript i is used to denote they represent ions. In the space weather model for the GEO environment utilized here, the ion species consists solely of protons. For high positive potentials, the ion current is very small because the ions are repelled by the positively charged spacecraft.

Charge control is achieved using an electron emitted from the tug onto the deputy. A portion of the beam current will be absorbed by the debris, depending on tug pointing accuracy and the charge levels of both tug and debris. This current is modeled as

$$I_D(\phi_D) = -\alpha I_t \qquad q\phi_T - q\phi_D < E_{EB} \qquad (4a)$$
$$= 0 \qquad q\phi_T - q\phi_D \geq E_{EB}, \qquad (4b)$$

where I_t is the beam current emitted by the tug, E_{EB} is the electron beam energy, and the subscripts T and D represent the tug and deputy, respectively. The parameter α represents the efficiency of the charge transfer process; it is the fraction of the beam current emitted by the tug that reaches the deputy. In general, this is a function of beam pointing accuracy and the width of the beam at the deputy location. It can also be impacted by the tug and debris potentials, in addition to the beam energy. In the current paper a value of $\alpha = 1$ is used, which maintains the value established in [29]. This assumes a well focused and accurately pointed beam. Better quantification of the α parameter is beyond the scope of this paper, and is left for future work. Once $\phi_T - \phi_D = E_{EB}$, it is impossible for additional beam current to make it to the deputy. The emitted beam electrons do not have enough energy to cross the potential difference between tug and deputy.

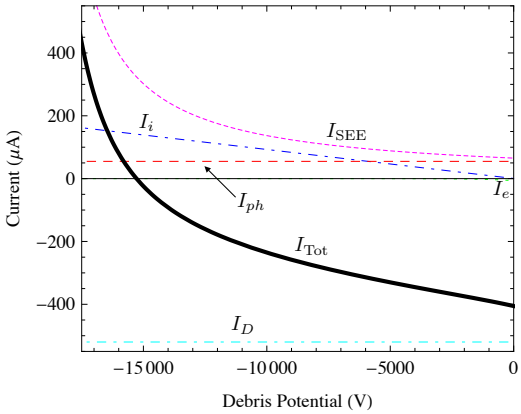

Fig. 4. Currents acting on the deputy for a range of deputy potentials. Deputy achieves a potential that results in I_{Tot}=0.

When the electron beam impacts the deputy object, the incoming electrons result in the emission of secondary electrons. Because of the large negative potential of the debris object (kV level), these electrons will escape. This represents a significant current source that must be accounted for. Secondary electron emission is modeled by[31]

$$I_{\text{SEE}}(\phi_D) = -4Y_M I_D(\phi_D)\kappa \qquad \phi_D < 0 \qquad (5a)$$
$$= 0 \qquad \phi_D \geq 0, \qquad (5b)$$

where

$$\kappa = \frac{E_{\text{eff}}/E_{\text{max}}}{(1 + E_{\text{eff}}/E_{\text{max}})^2}$$

and $E_{\text{eff}} = E_{EB} - q\phi_T + q\phi_D$. Y_M is the maximum yield of secondary electron production, and E_{max} is the impact energy at which this maximum occurs. In this paper, the values of $Y_M = 2$ and $E_{\text{max}} = 300$ eV are used.

For the tug, the charging is dominated by the plasma electron current and electron beam emission. The tug settles to a potential that satisfies the current balance $I_e(\phi_T) + I_t = 0$. This is solved analytically as

$$\phi_T = \left(\frac{4I_t}{Aqn_e w_e} - 1\right) T_e, \qquad (6)$$

which assumes a positive tug potential. This will be the case provided the beam current is sufficient. The current balance on the deputy object contains a few more contributions, and an analytical solution does not exist. The deputy will achieve

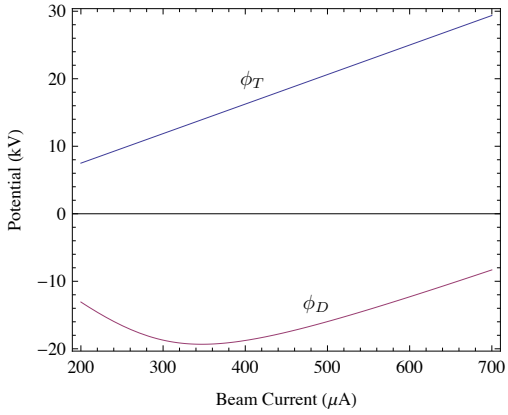

Fig. 5. Tug and deputy potentials as a function of beam current.

a potential that satisfies

$$I_{\text{Tot}} = I_e(\phi_D) + I_i(\phi_D) + I_{\text{SEE}}(\phi_D) + I_{ph}(\phi_D) + I_D(\phi_D) = 0. \quad (7)$$

The presence of the photoelectron current implies the deputy is in the sunlight. When in the Earth's shadow, the current balance contains all of the same terms except for I_{ph}. A numerical root finder is used to solve for ϕ_D in Eq. (7).

An example charging scenario is presented in Figure 4. Shown are the various currents impacting deputy charging for space weather conditions of $n_e = 0.6$ cm^{-3}, $n_i = 9.5$ cm^{-3}, $T_i = 50$ eV, and $T_e = 1250$ eV. The results assume a beam energy of E_{EB} =40 keV and a beam current of I_t=520 μA. The tug and deputy are treated as spheres, with radii of $r_T = 2$ m and $r_D = 0.935$ m. With these conditions, the tug achieves a potential of $\phi_T = 21.5$ kV and the deputy reaches a potential of $\phi_D = -15.3$ kV. As seen in Figure 4, the deputy potential results in a net zero current balance, i.e. $I_{\text{Tot}} = 0$. While the plasma electron current is included in the current balance, for the deputy it provides an insignificant contribution to charging at the high potential levels achieved. The tug and deputy potentials as a function of beam current are shown in Figure 5. The tug potential increases linearly with beam current, while the deputy potential has its largest value around $I_t = 350$ μA.

There are two electron beam parameters that may be used to influence charging: the beam energy and potential. Generally, a higher beam energy will result in higher deputy charging. This is due to the reduced secondary electron emission that stems from the higher energy of the incoming beam electrons. As the energy of an absorbed electron increases, fewer secondary electrons are emitted. Because the secondary electrons essentially result in the loss of some fraction of the incoming beam current, reducing the number of secondary electrons emitted will improve deputy charging. Depending on the space weather conditions, increasing or decreasing the beam current can improve or worsen deputy charging, as shown in Figure 5. However, the tug will always charge to higher potentials as the beam current is increased, up to the level of the beam energy ($q\phi_T \leq E_{EB}$).

B. Electrostatic Force Model

The performance of the electrostatic tug is dependent on the electrostatic force in place between the tug and deputy. To allow for analytic expressions, the tug and deputy object are treated geometrically as spheres, and are assumed to be perfectly conducting. The potential on the tug object is a result of its own charge and the potential due to the charged deputy object as[18]

$$\phi_T = k_c \frac{q_T}{r_T} + k_c \frac{q_D}{\rho}, \quad (8)$$

where $k_c = 8.99 \times 10^9$ Nm^2/C^2 is the Coulomb constant, ρ is the distance between tug and deputy, q_T is the charge on the tug, q_D is the charge on the deputy, and r_T is the radius of the tug craft. Similarly, the potential on the deputy object is computed as

$$\phi_D = k_c \frac{q_D}{r_D} + k_c \frac{q_T}{\rho}, \quad (9)$$

where r_D is the radius of the deputy object.

If the potentials on the tug and deputy are controlled, then the above relationships may be rearranged to solve for charge,[18]

$$\begin{bmatrix} q_T \\ q_D \end{bmatrix} = \frac{\rho}{k_c(\rho^2 - r_T r_D)} \begin{bmatrix} r_T\rho & -r_T r_D \\ -r_T r_D & r_D\rho \end{bmatrix} \begin{bmatrix} \phi_T \\ \phi_D \end{bmatrix}. \quad (10)$$

After computing the charges, the electrostatic force between tug and deputy is computed using

$$F_c = k_c \frac{q_T q_D}{\rho^2}. \quad (11)$$

Due to the space weather environment, some shielding of this electrostatic force will occur. The distance over which this shielding is prevalent is described by the Debye length of the local plasma.[32] The space weather conditions considered in this study yield Debye lengths that are on the order of tens of meters. However, because of the high potential levels obtained by tug and deputy, the Debye shielding effect will be several times smaller than predicted by the standard Debye length calculation. As discussed in [6] and [33], objects charged to tens of kiloVolts in the space environment experience effective Debye lengths several times larger. Looking specifically at this phenomenon as it pertains to charging in quiet GEO space weather conditions, the effective Debye lengths are predicted to be roughly 5 times larger than the classic Debye shielding model predicts.[33] The shortest Debye lengths considered here are on the order of 15 meters or more, leading to effective Debye lengths over 75 meters. This means that the space weather environment will not contribute significant shielding of the electrostatic force below distances of 75 meters. Because the separation distances considered here are less than 20 meters, the impacts of Debye shielding are insignificant and will not be included in the force model.

The ultimate goal of the electrostatic tractor is to raise the deputy orbit enough to reach a disposal orbit. The size of the deputy orbit is characterized by its semi-major axis, and reaching a disposal orbit requires an increase in the deputy

semi-major axis of 200-300 km. Assuming a circular deputy orbit, the semi-major axis increase in the deputy orbit over one day is[7]

$$\Delta a \approx \frac{4\pi}{n^2}\frac{F_c}{m_D}, \tag{12}$$

where n is the mean motion of the deputy orbit and m_D the deputy mass. A GEO orbit radius of 42,164 km is assumed for this analysis. The deputy mass is required to compute the semi-major axis change. Considering publicly available data on GEO satellites, [18] provides a relationship between spacecraft mass and an approximate sphere radius. The simple linear expression

$$r_D(m_D) = 1.152 \text{ m} + 0.00066350\frac{\text{m}}{\text{kg}}m_D \tag{13}$$

provides a deputy radius for use in the charging model. While certainly not perfect, this linear relationship does capture the general trend of increased mass for larger objects and is based on actual data for GEO objects.

III. Impact of Geomagnetic Storm Events on Tractor Performance

In [27] electrostatic tractor performance is analyzed for quiet ($k_p = 1.5$) geomagnetic storm conditions. Here the effects of geomagnetic storm events are considered. When a geomagnetic storm occurs, the population of lower energy ions (1-100 eV) in the period following local midnight is lost, with a higher energy population of slightly lower density (1 cm^{-3}) remaining.[24], [34] Solar storm events also provide a higher energy population of electrons, with energies as high as a few tens of keV. This phenomenon was experienced by the ATS-5 satellite and recorded in GEO space weather measurements taken by the magnetospheric plasma analyzer (MPA) instruments flown by Los Alamos National Laboratory.[35] When a spacecraft enters into eclipse during a storm event it may naturally charge to potential levels in excess of -10 kV, depending on the severity of the geomagnetic storm. During storm events experienced by ATS-5, typical potentials achieved in shadow were 3-4 kV (negative polarity), with lows of 70-100 V and highs in above 10 kV.[34] Note that a spacecraft experiences eclipse for under an hour each day in the 3-4 weeks before and after an equinox. Over an electrostatic tractor reorbiting scenario with a deorbit time of several months, this represents a very small portion of the total operating time. When a spacecraft is in sunlight, the photoelectron current precludes these very high natural charging levels. ATS-5 observed a maximum potential of -300 V in the sunlight, and reached potentials of between -50 and -300 V several times. All of these charging events occurred during periods of very high solar activity, and occurred between local midnight and dawn. The SCATHA satellite was also used to study natural charging in sunlight, and recorded potentials as high as -740 V.[36] Charging events in excess of -100 V only occurred for k_p indices of 2 or greater.

The NOAA space weather scale classifies the severity and frequency of geomagnetic storms, with a scale ranging from G-1 (minor, $k_p = 5$) to G-5 (extreme, $k_p = 9$).[26] In an 11 year solar cycle, minor storm activity is expected for roughly 900 days, with extreme storm events occurring much less frequently, only about 4 times. For the analysis of storm activity, two storm conditions are considered: a moderate geomagnetic storm, G-2 on the NOAA scale, with $k_p = 6$ and a worst-case severe storm event. Only the effects on the charge transfer process are considered. Severe solar activity can be harmful to spacecraft subsystems, causing electrical failures and differential charge driven arcing events, but consideration of these phenomena is beyond the scope of the current work. For the moderate storm condition ($k_p = 6$), data from [24] are used to determine plasma temperatures and densities. The data are taken at a local time of 3:00, which corresponds to the post-midnight period where high natural charging is observed. For the severe storm condition, the plasma parameters corresponding to a severe storm in [37] are used. The ion and electron densities for both storm conditions are presented in Table I, along with the quiet ($k_p = 1.5$) conditions computed for 3:00 local time using the data in [24].

TABLE I
Plasma parameters used for geomagnetic storm analysis

Storm Level	n_e (cm^{-3})	T_e (keV)	n_i (cm^{-3})	T_i (keV)
Moderate ($k_p = 6$)	1	4.7	1	15
Severe ($k_p = 8-9$)	1	20	1	20
Quiet ($k_p = 1.5$)	0.925	2.64	3.05	0.05

To determine the effects of these storm conditions, the tug and deputy potentials are computed as a function of electron beam current, for $E_{EB} = 40$ keV, $r_T = 2$ m, and $r_D = 0.935$ m. The electrostatic force is also computed, assuming a separation distance of 12.5 m. The potentials and forces are also computed for the quiet solar conditions ($k_p = 1.5$) to serve as a baseline for comparison. For the moderate solar storm event ($k_p = 6$), the results are illustrated in Figure 6. Also shown are potentials computed using the quiet conditions. The storm conditions result in the tug charging to higher potentials for a given electron beam current. For the deputy, the maximum potential occurs at a lower beam current level, and the potential decreases at a faster rate as the beam current is increased. The tug reaches its maximum potential ($q\phi_T = E_{EB}$) at a lower current level than for quiet space weather conditions. Considering the electrostatic forces that result, a slightly higher maximum force occurs for the storm condition and it occurs at a lower beam current level. The potentials and forces are also computed for the severe storm conditions, and are shown in Figure 7. The same effects are observed that are seen for moderate storm conditions, but to a higher degree. The tug potential increases more rapidly as beam current is increased, and the deputy potential decreases in a similar fashion. For the severe storm condition, the tug reaches its maximum potential for a beam current of about 575 μA, while in the moderate storm condition the tug potential is at its maximum for a beam current of almost 900 μA. As the storm severity increases, less current is required to maximally charge the tug. Looking at the electrostatic forces for the severe storm

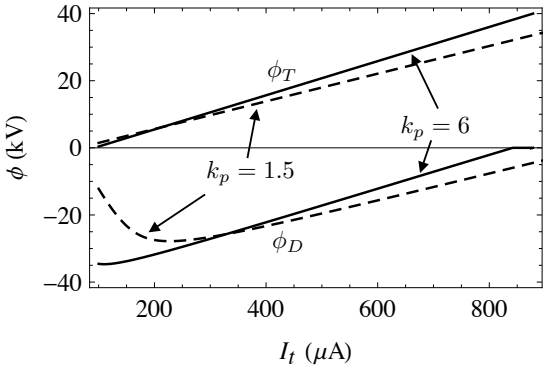

(a) Potentials

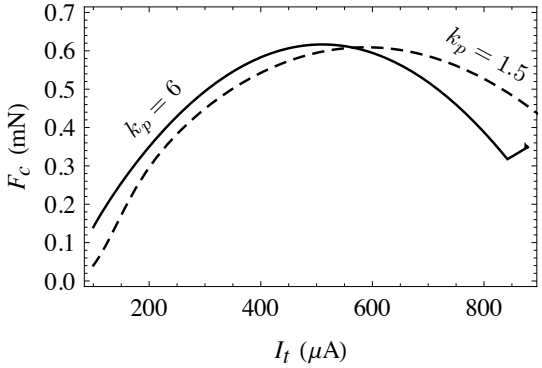

(b) E-Force

Fig. 6. a) Potentials and b) electrostatic force as a function of electron beam current for moderate solar storm event (solid) and quiet solar conditions (dashed). Results assume $r_T = 2$ m, $r_D = 0.935$ m, and $E_{EB} = 40$ keV.

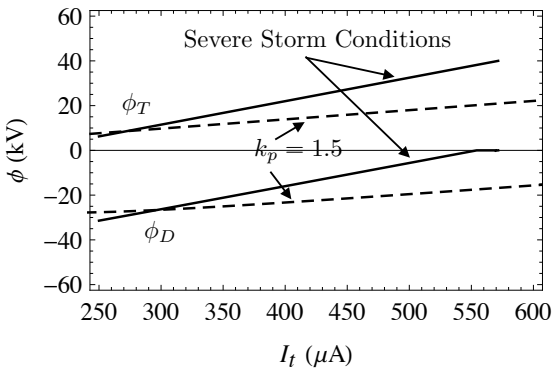

(a) Potentials

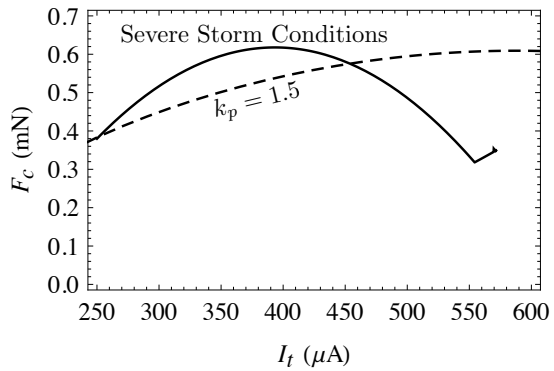

(b) E-Force

Fig. 7. a) Potentials and b) electrostatic force as a function of electron beam current for severe solar storm event (solid) and quiet solar conditions (dashed). Results assume $r_T = 2$ m, $r_D = 0.935$ m, and $E_{EB} = 40$ keV.

condition, the maximum is once again slightly above that of the quiet condition, but occurs at much less current.

Clearly, geomagnetic storm events do not prevent charge transfer for the electrostatic tractor. In fact, they are actually somewhat helpful. A slightly higher electrostatic force is possible, and less current is required to achieve it. Current modification is required to compensate for the onset of these storm events, however. When considering the nominal GEO space weather conditions for quiet periods of activity, the maximum electrostatic force occurs for a beam current of nearly 600 μA. If a severe solar storm event occurs and the beam current is not modified to compensate, Figure 7 shows that the tug will reach its maximum potential ($q\phi_T = E_{EB}$), preventing charge transfer and significantly impacting performance. Thus, to account for solar storm events the beam current should be controllable, which is likely to be the case anyway. The analysis of solar storm events on tractor performance reveals that the worst-case scenario from a performance perspective is actually the nominal, quiet space weather conditions. For this reason, quiet storm conditions are assumed for further studies.

IV. Tug Electron Back-Flux

Two deputy current sources are due to emission of electrons from the deputy surface: photoelectron and secondary electron emission. Because the deputy is charged negatively, these electrons are lost. The nearby tug, however, recaptures a portion of these emitted electrons, as depicted in Figure 8, owing to high positive potential. This serves as an additional current source on the deputy object which will impact its charging. Thus, it is important to study this effect, and obtain a rough estimate for how significantly these current sources affect tug charging. The scope of this analysis is not meant to be comprehensive, but rather to provide some insight into how much this back-flux might affect electrostatic tractor performance. A two meter

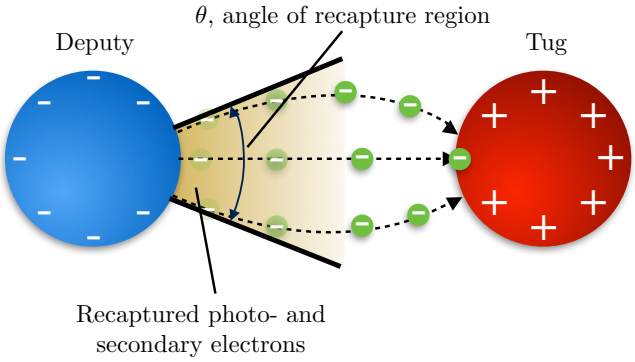

Fig. 8. Electron back-flux from the deputy to the tug.

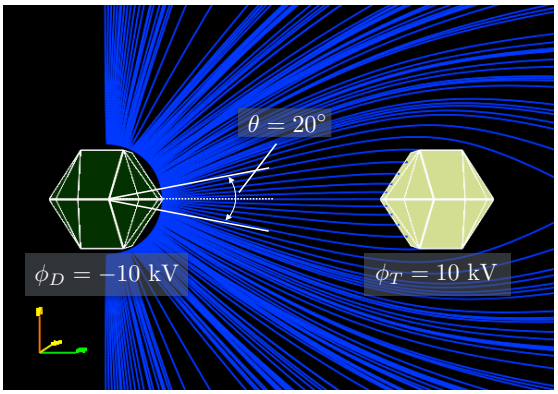

(a) $\phi_T = -\phi_D = 10$ kV

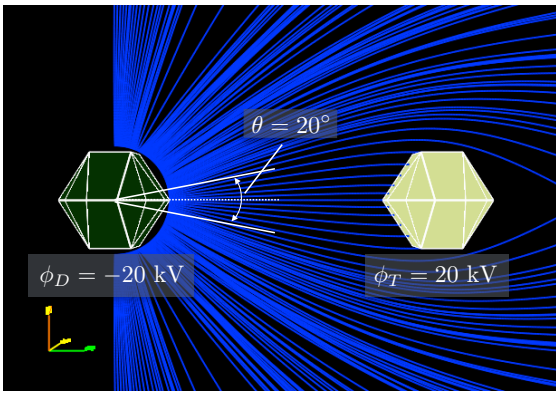

(b) $\phi_T = -\phi_D = 20$ kV

Fig. 9. Electron back-flux trajectories computed by NASCAP-2K for a) $\phi_T = -\phi_D = 10$ kV and b) $\phi_T = -\phi_D = 20$ kV. Results assume spheres of two-meter radius separated by a distance of 12 meters.

radius is assumed for both tug and deputy and the quiet space weather conditions at 17:30 local time are used, corresponding to $n_e = 0.47$ cm^{-3}, $T_e = 1180$ eV, $n_i = 11$ cm^{-3}, $T_i = 50$ eV.[24] These values are chosen to represent the worst-case charge transfer performance conditions, as observed in [27].

To identify the angle of the recapture region, θ, the NASCAP-2K spacecraft charging analysis software is used.[38] Developed by NASA and the Air Force Research Lab, NASCAP-2K is capable of simulating charging behavior of 3-D spacecraft models, computing potentials in space, and tracking particle trajectories. To identify the region of recapture, potentials are prescribed onto two spherical objects (each with two-meter radius) separated by a distance of 12 meters. NASCAP-2K is then used to compute the potentials in space around the objects. Following this computation, electrons are distributed around the deputy object with a temperature of 2 eV. These electrons may represent either secondary or photoelectrons, as both are emitted at low energy. The electron trajectories are then computed to determine if they are recaptured by the tug vehicle. Two particular cases are considered: $\phi_T = -\phi_D = 20$ kV and $\phi_T = -\phi_D = 10$ kV.

The resulting electron trajectories are shown in Figure 9. The region of recapture for the 10 and 20 kV equal potential

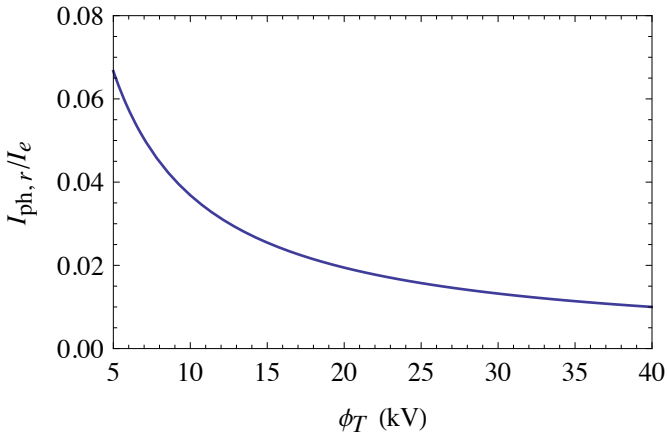

Fig. 10. Ratio of recaptured photoelectron current and tug plasma electron current for two meter tug and deputy radii.

cases is nearly identical, with $\theta = 20°$. Any electrons emitted within this region will be recollected by the tug, constituting an additional current source that will affect tug charging. If the electron beam is directed along the line of sight from tug to deputy and is sufficiently narrow when it reaches the deputy, a very large portion of the resulting secondary electrons may be recaptured by the tug. Depending on the potential levels of tug and deputy, the secondary electron current can be a significant fraction of the beam current. In order to avoid the recapture of these electrons, a very narrow electron beam may not be the best choice. Alternately, the electron beam could be focused onto an area outside the region of recapture.

The back-flux of photoelectrons is an additional current source onto the tug. Assuming a worst-case scenario where the sun shines directly onto the region of recapture, the maximum cross sectional area for which emitted photoelectrons are recaptured is

$$A_\perp = \pi r_D^2 \sin^2\left(\frac{\theta}{2}\right). \tag{14}$$

This is a higher area than could physically be exposed to sunlight because the tug would shadow at least some portion of the deputy. Assuming the tug is at potential levels of at least a few kiloVolts, the magnitude of this recaptured photoelectron current is insensitive to further increases in electron beam current. The recaptured photoelectron current is expressed as

$$I_{ph,r} = -\pi j_{ph} r_D^2 \sin^2\left(\frac{\theta}{2}\right). \tag{15}$$

To provide insight into how significant this current is on the tug, it is compared with the collected plasma electron current (I_e). Using the value of $\theta = 20°$ determined from the NASCAP-2K simulations, the ratio of recaptured photoelectron current to plasma electron current is shown in Figure 10. For the tug potentials considered for the electrostatic tractor application, the recaptured photoelectron current is a very small fraction (5% or less) of the incoming plasma electron current. Thus, this effect will not significantly impact the

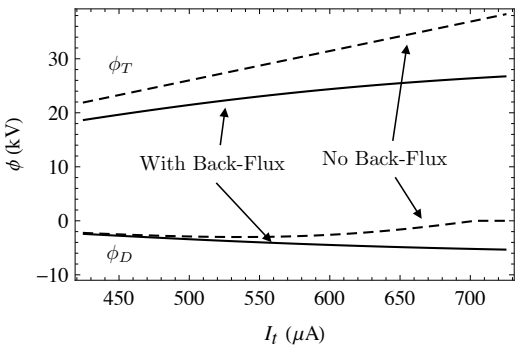

(a) Potentials

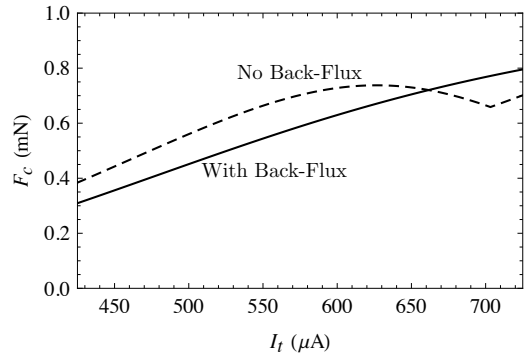

(b) Electrostatic Force

Fig. 11. a) Tug and deputy potentials with and without electron back-flux onto the tug and b) resulting electrostatic forces.

charging of the tug. The tug vehicle can simply emit slightly more current to offset these recaptured photoelectrons.

Assessing the impacts of recaptured secondary electrons is somewhat more complicated, because the recaptured SEE current depends on how well focused the beam is and how much beam current is absorbed by the deputy. Assuming a worst case scenario where all secondary electrons are recaptured by the tug, the potentials ϕ_T and ϕ_D are found by solving

$$I_t + I_e(\phi_T) - I_{\text{SEE}}(\phi_T, \phi_D) + I_{ph,r} = 0 \tag{16a}$$

$$I_D(\phi_T, \phi_D) + I_e(\phi_D) + I_i(\phi_D) + I_{\text{SEE}}(\phi_T, \phi_D) + I_{ph} = 0. \tag{16b}$$

In the absence of back-flux, the tug potential is not a function of the deputy potential and can be solved directly. With back-flux, however, the tug potential is a function of the deputy potential due to the recaptured secondary electrons and these two current balance equations must be solved simultaneously for ϕ_T and ϕ_D. Considering the same 2 meter radius tug and deputy objects, at a separation distance of 12 meters, the potentials as a function of electron beam current are computed and shown in Figure 11. Also shown for comparison are the charging results if back-flux is neglected (or nonexistent). With back-flux, the tug and deputy potentials both increase as the electron beam is increased. Without back-flux, the tug potential increases linearly; the deputy potential increases up to a certain point and then begins to decrease. The presence of back-flux results in potential changes of several kiloVolts. The tug potential is lower than without back-flux, while the deputy potential is higher. The resulting electrostatic forces are also shown in Figure 11. For lower current values, the electrostatic force is reduced by the back-flux. However, there is a certain current level beyond which the electrostatic force is higher with back-flux than without it.

The recaptured electrons reduce the tug potential for a given electron beam current. This allows for more current to be sent to the deputy at a higher energy level. The beam electrons lose less energy because the potential difference between tug and deputy is reduced by the back-flux. Because they arrive with more energy, the beam electrons induce fewer secondary electrons. This allows for the deputy to reach a higher potential, which can improve tractor performance at the cost of higher electron beam current. This phenomenon is driven primarily by the recaptured secondary electrons, because this current source is significantly larger than the small portion of photoelectrons that are recaptured. Of course, this analysis assumes a worst case scenario where all secondary electrons emitted by the deputy are recaptured by the tug, which depends on how well-focused the beam is and where it is absorbed on the deputy. As a smaller portion of electrons are recaptured, the charging results approach those with no back-flux.

V. Simultaneous Electron/Ion Beam Emission

Deputy charging is limited by the amount of current that can be delivered to it by the tug. As the tug emits more electron beam current, it will charge itself to higher potentials. This results in the beam electrons having lower energy when they reach the deputy, generally causing a higher secondary electron yield. Thus, the deputy charging can actually decrease even for higher beam currents, as illustrated in Figure 5. Furthermore, the plasma electron conditions can cause the tug to charge up to relatively high values and limit the deputy potential. This can cause significant deviations from the ideal potential split, leading to reduced performance. These performance losses are encountered in the analysis of space weather variations on tugging performance studied in [27]. A dip in electron density after local noon results in a higher tug potential for a given beam current, which in turn results in a lower deputy potential.

It would be very beneficial if the tug could change the amount of current delivered to the deputy without affecting its own potential. If a tug vehicle could maintain, for example, a 20 kV potential while emitting a broad range of electron beam currents, deputy charging could be improved and the tug vehicle would be able to perform charge transfer onto a wider variety of deputy sizes. With only electron beam emission, of course, this is impossible. However, consider a scenario where the tug is equipped not only with an electron gun, but also an ion beam. Assuming the ion beam is directed away from the deputy object in a manner that does not result in an additional current source on the deputy, the deputy charging dynamics would be the same as in Eq. (7). Assuming there is sufficiently more electron beam current than ion beam current so that the

tug charges to a high positive potential, the tug current balance takes on the slightly modified form

$$I_t - I_b + I_e(\phi_T) = 0, \tag{17}$$

where I_b is the ion beam current. Note that electron back-flux is ignored here. This may be accomplished with a defocused electron beam, or by focusing the electron beam away from the region of recapture. The tug potential, then, is a function of the net emitted current $\Delta I_B = I_t - I_b$:

$$\phi_T = \left(\frac{4\Delta I_B}{Aqn_e w_e} - 1 \right) T_e \tag{18}$$

The tug vehicle, being charged positive, will not recapture the beam ions in any significant capacity.

With the ion beam, a tug vehicle can theoretically emit any amount of electron beam current while maintaing a specific potential. For example, if the tug is desired to maintain a potential of 20 kV with a ΔI_B of 500 μA, any amount of electron beam current above 500 μA may be delivered to the deputy. If 1000 μA of electron beam current is emitted, then 500 μA of ion beam current must also be emitted to maintain the necessary ΔI_B.

The ion beam emission allows for performance improvement in a variety of ways. Revisiting the issue of tug/deputy size limitations, a tug would be able to achieve charge transfer onto objects larger than itself. With only an electron beam, the amount of beam current that the tug can emit is limited by the tug size. As the tug emits more current, it charges to a higher potential. The beam electrons that reach the deputy have a lower effective energy when they arrive, resulting in further performance losses due to higher secondary electron emission. With an ion beam included, however, the tug can now deliver the necessary amount of electron beam current for deputy charging. Emitting higher levels of electron beam current does not necessarily result in higher tug potentials, because ion beam current can be increased to maintain a constant tug potential. More current can be delivered to the deputy at higher energies, inhibiting losses due to secondary electron emission. Considering the space weather driven performance losses encountered in [27], the increase in tug potential in the afternoon period can be eliminated by compensation with the ion beam. Keeping the tug potential from increasing also prevents the deputy potential from decreasing. The end result is that both potentials remain close to the ideal split, where best performance occurs.

Naturally, simultaneous beam emission raises the question of what current emission strategy will yield the best performance for the electrostatic tractor. To provide insight into the effects of increasing electron and ion beam currents on the resulting electrostatic force, a numerical optimization is used. Considering a range of emitted ion beam currents, the maximum possible electrostatic force and its associated electron beam current are computed. The quiet GEO space weather conditions at 17:30 are, again, used. Both tug and debris are assumed to have radii of two meters, and the electron beam energy is assumed to be 40 keV. The ion beam current is swept across a range of values, and the maximum possible electrostatic force is computed, along with the ΔI_B need to achieve the max force. The results are shown in Figure 12. As the ion and, correspondingly, electron beam currents are increased, the maximum electrostatic force increases. However, there is a limit on the increase, regardless of how much current is emitted. This reflects the fact that for a given beam energy, the maximum potential difference between tug and deputy is finite. Furthermore, as the current is increased the ideal ΔI_B also converges towards a distinct value. Here, the inclusion of an ion beam allows for a significant boost in the electrostatic force magnitude. With only electron beam emission (I_b = 0), the maximum electrostatic force that can be generated is just under 0.8 mN. As the ion and, correspondingly, electron beam currents are increased, the maximum electrostatic force increases towards a limit of slightly less than 1.5 mN. This is an an increase of 87%, which would nearly cut the reorbiting time required in half.

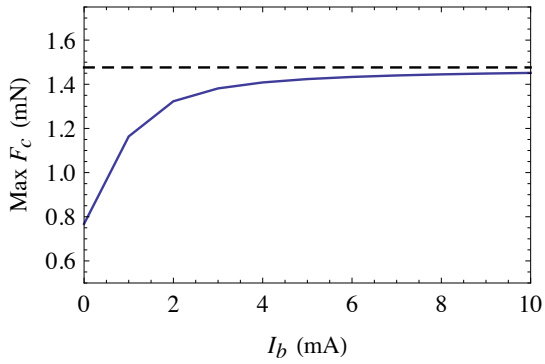

(a) Maximum E-Force

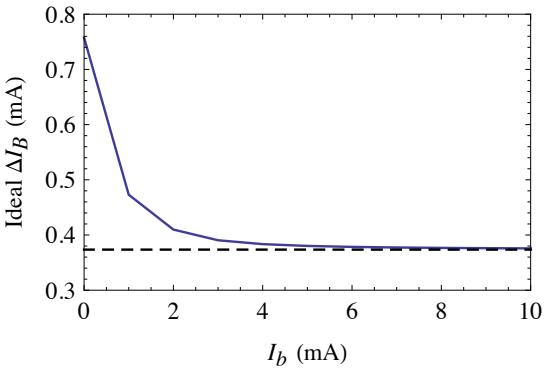

(b) Ideal ΔI_B

Fig. 12. a) Maximum possible electrostatic force and b) ΔI_B required to obtain the maximum force for simultaneous electron and ion beam emission. Dashed lines are the limiting values for the case of very large current emission. The results are computed with $r_T = r_D = 2$ m and $E_{EB} = 40$ keV.

These results imply that for the case of simultaneous electron and ion beam emission, delivering ever higher amounts of current to the deputy will yield the best tractor performance. Clearly, though, there is a limit to how large of an electrostatic force may be generated, even for very high current levels. The only non-beam deputy current source that increases directly

as a function of the electron beam current is the secondary electron current. As the beam current is increased to very high values, the ion and photoelectron currents become insignificant relative to the secondary electron and beam absorption currents. Thus, the deputy will reach a potential that satisfies

$$I_D - 4Y_M I_D \kappa = 0. \tag{19}$$

The deputy potential that satisfies this current balance is

$$\phi_D = \phi_T - E_{EB} + E_{\max}(2Y_M - 1) + 2E_{\max}\sqrt{Y_M(Y_M - 1)}. \tag{20}$$

The maximum secondary electron yield Y_M must be greater than one for a real solution to exist. If the max yield were below 1, the secondary electrons would be unable to balance with the incoming beam current and the deputy would settle to a potential difference such that $q\phi_T - q\phi_D = E_{EB}$. With simultaneous electron and ion beam emission, the largest theoretical difference that is possible between tug and deputy is $E_{EB} - E_{\max}(2Y_M - 1) + 2E_{\max}\sqrt{Y_M(Y_M - 1)}$. The losses in efficiency due to secondary electron emission are apparent.

To compute the maximum possible force with electron/ion beam emission, the cost function

$$J = (r_D\phi_D - \rho\phi_T)(\rho\phi_D - r_T\phi_T) \tag{21}$$

is used. This comes directly from the electrostatic force expression, and the electrostatic force is at its largest magnitude when J is maximized. After substituting in Eq. (20) for ϕ_D, and setting $\partial J/\partial\phi_T = 0$, the tug potential that will yield that maximum force is found to be

$$\phi_T^* = \frac{E_{EB} - E_{\max}\left(2Y_M - 1 + 2\sqrt{Y_M(Y_M-1)}\right)}{2} \times \frac{\rho^2 - 2\rho r_D + r_D r_T}{(\rho - r_D)(\rho - r_T)}. \tag{22}$$

Similarly, the deputy potential at the maximum force condition is

$$\phi_D^* = -\frac{E_{EB} - E_{\max}\left(2Y_M - 1 + 2\sqrt{Y_M(Y_M-1)}\right)}{2} \times \frac{\rho^2 - 2\rho r_T + r_D r_T}{(\rho - r_D)(\rho - r_T)}. \tag{23}$$

The ΔI_B required to provide the necessary ϕ_T^* is

$$\Delta I_B^* = \frac{Aqn_e w_e}{4}\left(1 + \frac{\phi_T^*}{T_e}\right). \tag{24}$$

This limit is plotted in Figure 12 for the scenario considered therein, and reflects the asymptote that the numerically computed result is approaching. The theoretical maximum force that can be generated with both ion and electron beam emission is

$$F_c = -\frac{r_D r_T}{4k_c(\rho - r_D)(\rho - r_T)}\left(E_{EB} + E_{\max}(1 - 2Y_M) - 2E_{\max}\sqrt{Y_M(Y_M-1)}\right)^2. \tag{25}$$

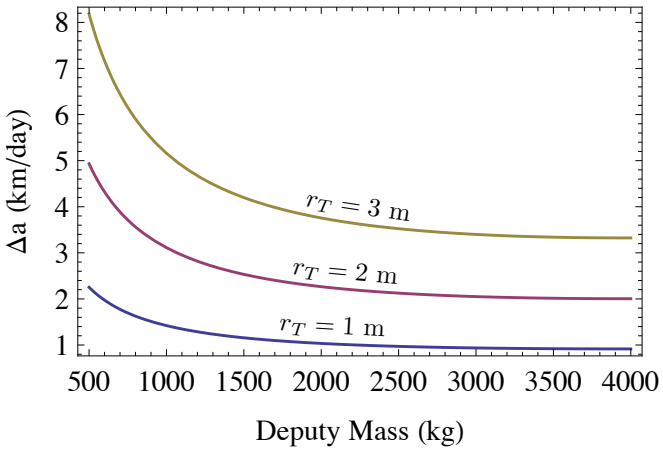

Fig. 13. Theoretical maximum semi-major axis increase per day for a range of tug and deputy masses with simultaneous electron and ion beam emission. Results assume $E_{EB} = 40keV$.

This limit is also plotted in Figure 12, and the numerically computed maximum forces approach it as the currents are increased.

Of course, emitting arbitrarily large currents is not physically possible for a number of reasons. In addition to very high power requirements, the maximum current is limited by the space charge effect. If the charge density in a beam is high enough, the mutual repulsion between similarly charged particles reduces the beam velocity and limits the current flow.[21] These results should not be interpreted as implying that arbitrarily large currents can be emitted for the electrostatic tractor application. Rather, they serve to provide an upper limit on the performance improvement that may be gained by including ion beam emission in addition to electron beam emission. Further, Figure 12 shows that, for the vehicle sizes considered here, the achievable electrostatic forces with milliamp level currents approach the theoretical maximum to within 10%. Electron beam currents in excess of 10 milliamps have been demonstrated in flight, and the SCATHA mission is one such example.[39]

The semi-major axis increases per day for a one, two, and three meter radius tug as a function of deputy mass are computed using the ideal electrostatic force expression in Eq. (25), assuming an electron beam energy of 40 keV and quiet space weather conditions at 17:30. The results are shown in Figure 13. The largest, three meter radius tug provides the best performance, towing objects of 4000 kg with a semi-major axis increase of more than 3 km/day. For the one meter tug, even simultaneous electron and ion beam emission is not enough to tow larger deputy objects at a rate of $\Delta a = 1$ km/day.

Considering the dual beam scenario, we address the question of the maximum towable deputy mass. To compute the maximum towable mass, the linear mass-radius relationship in Eq. (13) is employed. Using the best-case electrostatic force predicted by Eq. (25) in conjunction with the approximate semi-major axis increase per day from Eq. (12) allows for a

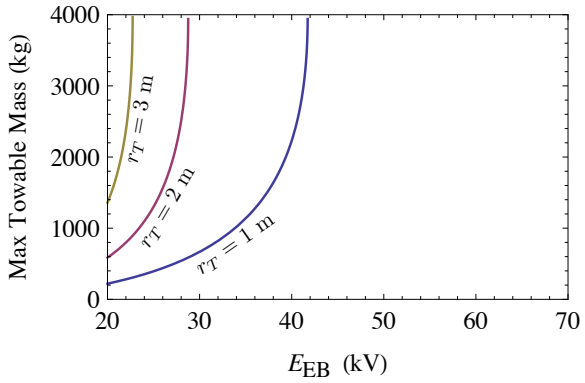

(a) Δa =1 km/day

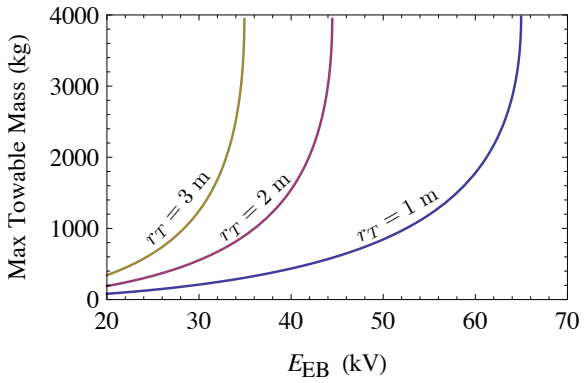

(b) Δa =2.5 km/day

Fig. 14. Maximum towable mass using simultaneous electron and ion beam emission to meet performance criteria of a) Δa = 1 km/day and b) Δa =2.5 km/day.

numerical solution of the deputy mass that will yield a desired Δa given a particular tug radius, separation distance, and electron beam energy. Two performance thresholds are used: Δa =1 km and Δa =2.5 km. The Δa =1 km performance level is somewhat lower than typically assumed, and for the debris reorbiting scenario would require a maneuver duration of roughly 7-10 months. The higher performance level of Δa =2.5 km is more typical of what has been assumed in prior electrostatic tractor research.[7]

The maximum towable masses as a function of electron beam energy are shown in Figure 14 for tug sizes of r_T =1, 2, and 3 meters. The improved performance for larger tug vehicles is apparent. Significantly less beam energy is needed to achieve the same level of performance for the three meter tug radius than for the one meter tug radius. By incorporating ion beam emission, a tug with a one meter radius can tow objects as large as 4000 kg at a rate of Δa =2.5 km/day with an electron beam energy of 65 keV. To achieve a Δa of 2.5 km/day, the three meter radius tug needs only 35 keV.

Ion beam emission, owing to the higher mass of ions relative to electrons, can impart a significant thrust force onto the tug vehicle. In fact, low-thrust propulsion systems have been designed around continuous ion emission.[40], [41], [42] Further, the ion-beam shepherd concept considers the use of

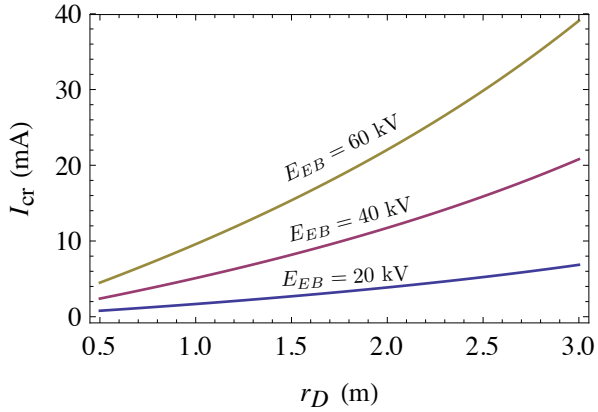

Fig. 15. Ion beam current for which F_{th} is equal to the maximum possible electrostatic force for simultaneous electron and ion beam emission.

a collimated ion beam to impart a small force onto a debris object due to the impact of the incoming ions on the debris object, which is used for deorbiting purposes.[43] For the case of simultaneous ion and electron beam emission, performance improves as more beam current is emitted. Because the ion thrust force increases as more current is emitted, there will be a point beyond which the thrust force is higher than the electrostatic force. Because the tug vehicle is charged to a high positive potential ions that are emitted will be repelled, so there is no need for a high energy ion beam. It is assumed that the ions are emitted in a direction that will not lead to their capture by the negatively charged deputy.

The thrust force on the tug due to the ion beam emission is

$$F_{th} = \frac{I_b}{q} m_b v_\infty(\phi_T) \tag{26}$$

where m_b is the mass of the ions and

$$v_\infty(\phi_T) = \sqrt{\frac{2q\phi_T}{m_b}} \tag{27}$$

is the velocity of the ions at infinity, after they have been accelerated out of the tug potential well. This formulation assumes that the ions are emitted with low energy, and that all of their v_∞ is due to acceleration by the tug's electric field. The ion species is assumed to be Argon (Ar^+), with an associated mass of $m_b = 6.63 \times 10^{-26}$ kg. The thrust force matches the performance limit for dual beam emission when

$$\frac{I_b}{q} m_b v_\infty(\phi_T^*) = -\frac{r_D r_T}{4k_c(\rho - r_D)(\rho - r_T)} \Big(E_{EB} + E_{\max}(1 - 2Y_M) - 2E_{\max}\sqrt{Y_M(Y_M - 1)} \Big)^2 . \tag{28}$$

Solving this equation for I_b yields the critical beam current, I_{cr}, for which more force is generated by the ion beam emission than is possible for the electrostatic attraction. Considering the case of a two meter tug radius, this critical current level is computed for electron beam energies of 20, 40, and 60 keV and presented in Figure 15. Higher beam energies allow for higher potentials on tug and deputy, resulting in a

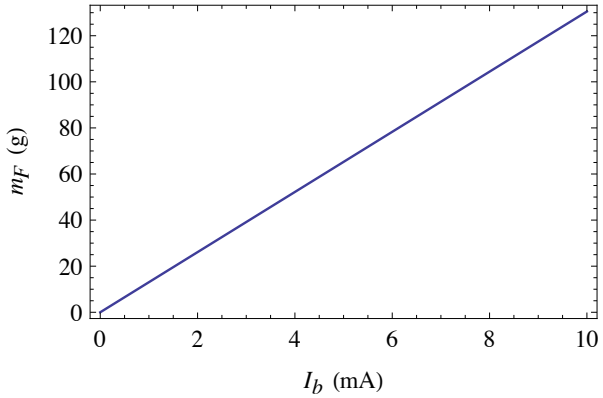

Fig. 16. Fuel required for continuous ion beam emission over the course of one year.

larger electrostatic force. Thus, it takes more ion beam current to generate equivalent levels of thrust. As r_D is increased, more charge accumulates on the deputy for the same potential level. This also results in a larger electrostatic force and a higher I_{cr} level. Depending on E_{EB} and the deputy size, only a few milliamps of current are required for the ion beam thrust to equal the maximum electrostatic force. As seen in Figure 12, it may take several milliamps of current before the electrostatic force magnitude begins to closely approach the theoretical maximum. This implies that actually achieving the potential increases that are possible with dual beam emission may result in a scenario where the ion beam thrust is on the same order of the electrostatic force. Considering again the scenario depicted in Figure 12, with a two meter tug and deputy radius, the electrostatic forces begin to closely approach the theoretical maximum around an ion beam current of 5-6 milliamps. Considering Figure 15, the amount of ion beam current required to reach the level of these electrostatic forces is 12 millamps. For this particular scenario, where roughly 5-6 milliamps of ion beam current are required to achieve maximum performance, the thrust due to the resulting ion beam emission is roughly half of the electrostatic force magnitude.

Operating the ion beam requires a consumable source of fuel for ion generation. The reorbiting times of several months means that the ion beam will have to be emitted continuously for a long duration. Thus, it is of interest to investigate roughly how much fuel is required for ion beam operation. The mass flow rate of fuel due to the ion beam is computed as

$$\dot{m}_F = \frac{I_b}{q} m_i. \tag{29}$$

Considering a continuous operating time of one year, the total fuel consumption for a range of ion beam currents is shown in Figure 16. For current levels of several milliamps, the total fuel consumption is about 130 g. Considering the sizes of the tug and deputy objects, this is a negligible increase in total system mass and not a significant hindrance for adding ion beam emission.

The decision to equip a tug vehicle with both an ion and electron beam depends on several factors. Really maximizing the benefits that are possible with simultaneous emission requires a large increase in the emitted beam current levels. This has a direct impact on the resulting power requirements. For a two meter tug with only an electron beam, the maximum power required for beam operation is driving the tug to its maximum potential ($q\phi_T = E_{EB}$), and is about 30 W. Maximizing performance benefits with an ion beam requires at least several milliamps of current. Estimating power requirements as $P = I_t E_{EB}$, emitting 6 milliamps of electron beam current with an energy of 40 keV requires 240 W. This is an increase of 700%, and does not even include additional power consumption due to the ion beam emission. Still, power generation in excess of 10 kW has been achieved in operating GEO satellites,[44] so this issue of increased power consumption is not likely to pose any significant technical hurdles.

Another practical concern is the additional complexity of adding a second current source (the ion beam). While it can greatly improve the performance for smaller tug vehicles where electron beam only charge transfer onto large deputy objects fails, this must be weighed against the decision to simply build a larger tug vehicle with only an electron beam. Increasing the size of the tug does not necessarily necessitate increased vehicle mass and higher launch costs. There are no requirements on tug density, so it could be built like a hollow shell, keeping the mass increases manageable for larger tug vehicles.

Lastly, the ion beam emission introduces a significant thrust force. While this does not preclude any functionality of the electrostatic tractor it is something that the relative motion control system will have to compensate for, increasing the required thrust for station keeping. If the ions are emitted directly away from the deputy object, a ion-beam thrust on the same order as the electrostatic will double the station-keeping thrust requirements. This will, in turn, double fuel requirements. It may be possible, however, to mitigate these effects somewhat by emitting the ions such that they provide some portion of the required station-keeping thrust. Doing so, however, would require emission in the direction of the deputy object. This could lead to recollection of the ions by the deputy, which would reduce deputy charging and hurt tractor performance. A full analysis of this phenomenon is beyond the scope of this study.

VI. Conclusion

The impacts of geomagnetic storm activity on charge transfer for the electrostatic tractor application are considered. While the variations in the plasma environment resulting from these storm events do affect the charging of tug and deputy, they can actually improve tractor performance. The tug must be able to compensate, however, by modifying electron beam current for the onset of such storms or performance will suffer. Both photoelectrons and secondary electrons are emitted from the deputy in the near vicinity of the positively charged tug.

Some of the electrons are recaptured by the tug, resulting in an additional current source. This back-flux also somewhat improves tractor performance by allowing the tug to deliver more current at a slightly higher energy to the deputy. Charge transfer performance can be improved by incorporating an ion beam onto a tug vehicle equipped with an electron beam. Simultaneous electron and ion beam emission allows the tug to deliver more electron current to the deputy while keeping its own potential from increasing. This allows the deputy to reach a higher potential and the tractor force may be significantly improved, especially for smaller tug vehicles where charge transfer fails with only an electron beam. Of course, this comes at the cost of higher power requirements and the added complexity of dual beam emission.

ACKNOWLEDGMENT

The authors would like to thank Zoltan Sternovsky for his input on the charging dynamics.

REFERENCES

[1] S. R. C. Ltd, "Space debris: On collision course for insurers?" http://media.swissre.com/documents/Publ11_Space+debris.pdf, Tech. Rep., March 2011.

[2] P. V. Anderson and H. Schaub, "Local orbital debris flux study in the geostationary ring," *Advances in Space Research*, vol. 51, no. 12, pp. 2195–2206, 2013. [Online]. Available: http://www.sciencedirect.com/science/article/pii/S0273117713000410

[3] ——, "Local debris congestion in the geosynchronous environment with population augmentation," *Acta Astronautica*, vol. 94, no. 2, pp. 619–628, Feb. 2014.

[4] "IADC space debris mitigation guidelines," Inter-Agency Space Debris Coordination Committee, Tech. Rep. IADC-02-01, 2007.

[5] "Nasa safety standard: Guidelines and assessment procedures for limiting orbital debris," National Aeronautics and Space Administration, Tech. Rep. NSS 1740.14, 1995.

[6] N. Murdoch, D. Izzo, C. Bombardelli, I. Carnelli, A. Hilgers, and D. Rodgers, "Electrostatic tractor for near earth object deflection," in *59th International Astronautical Congress, Glasgow, Scotland*, vol. 29, 2008.

[7] H. Schaub and D. F. Moorer, "Geosynchronous large debris reorbiter: Challenges and prospects," *The Journal of the Astronautical Sciences*, vol. 59, no. 1&2, pp. 165–180, 2012.

[8] E. Hogan and H. Schaub, "Relative motion control for two-spacecraft electrostatic orbit corrections," *AIAA Journal of Guidance, Control, and Dynamics*, vol. 36, no. 1, pp. 240–249, Jan. – Feb. 2013.

[9] Y. S. Karavaev, R. M. Kopyatkevich, M. N. Mishina, G. S. Mishin, P. G. Papushev, and P. N. Shaburov, "The dynamic properties of rotation and optical characteristics of space debris at geostationary orbit," in *Advances in the Astronautical Sciences*, vol. 119, 2004, pp. 1457–1466, Paper No. AAS-04-192.

[10] P. Couzin, F. Teti, and R. Rembala, "Active removal of large debris: Rendezvous and robotic capture issues," in *2nd European Workshop on Active Debris Removal*, Paris, France, 2013, paper No. 7.5.

[11] L. B. King, G. G. Parker, S. Deshmukh, and J.-H. Chong, "Spacecraft formation-flying using inter-vehicle coulomb forces," NASA/NIAC, http://www.niac.usra.edu, Tech. Rep., January 2002.

[12] H. Schaub and D. Stevenson, "Prospects of relative attitude control using coulomb actuation," in *Jer-Nan Juang Astrodynamics Symposium*, College Station, TX, June 25–26 2012, Paper AAS 12–607.

[13] D. Stevenson and H. Schaub, "Multi-sphere method for modeling electrostatic forces and torques," *Advances in Space Research*, vol. 51, no. 1, pp. 10–20, Jan. 2013.

[14] P. Couzin, F. Teti, and R. Rembala, "Active removal of large debris: System approach of deorbiting concepts and technological issues," in *6th European Conference on Space Debris*, Darmstadt, Germany, April 22–25 2013, paper No. 6a.P-17.

[15] A. Natarajan and H. Schaub, "Linear dynamics and stability analysis of a coulomb tether formation," *Journal of Guidance, Control, and Dynamics*, vol. 29, no. 4, pp. 831–839, July–Aug. 2006.

[16] I. I. Hussein and H. Schaub, "Invariant shape solutions of the spinning three craft coulomb tether problem," *Journal of Celestial Mechanics and Dynamical Astronomy*, vol. 96, no. 2, pp. 137–157, 2006.

[17] S. Wang and H. Schaub, "Nonlinear charge control for a collinear fixed shape three-craft equilibrium," *AIAA Journal of Guidance, Control, and Dynamics*, vol. 34, no. 2, pp. 359–366, Mar.–Apr. 2011.

[18] H. Schaub and L. E. Z. Jasper, "Orbit boosting maneuvers for two-craft coulomb formations," *AIAA Journal of Guidance, Control, and Dynamics*, vol. 36, no. 1, pp. 74–82, Jan. – Feb. 2013.

[19] U. Yamamoto and H. Yamakawa, "Two-craft coulomb-force formation dynamics and stability analysis with debye length characteristics," in *AIAA/AAS Astrodynamics Specialist Conference and Exhibit*, Honolulu, Hawaii, Aug. 18–21 2008, paper No. AIAA 2008-7361.

[20] L. Felicetti and G. B. Palmerini, "Evaluation of control strategies for spacecraft electrostatic formation keeping," in *IEEE Aerospace Conference*, Big Sky, MO, Mar. 1–8 2014, paper No. 2.0904.

[21] S. T. Lai, *Fundamentals of Spacecraft Charging*. Princeton University Press, 2012.

[22] T. Nakagawa, T. Ishii, K. Tsuruda, H. Hayakawa, and T. Mukai, "Net current density of photoelectrons emitted from the surface of the geotail spacecraft," *EARTH PLANETS AND SPACE*, vol. 52, no. 4, pp. 283–292, 2000.

[23] M. C. Kelley, *The Earth's Ionosphere: Plasma Physics & Electrodynamics*. Academic press, 2009, vol. 96.

[24] M. H. Denton, M. F. Thomsen, H. Korth, S. Lynch, J. C. Zhang, and M. W. Liemohn, "Bulk plasma properties at geosynchronous orbit," *Journal of Geophysical Research*, vol. 110, no. A7, 2005.

[25] J. Bartels, N. H. Heck, and H. F. Johnston, "The three-hour-range index measuring geomagnetic activity," *Terrestrial Magnetism and Atmospheric Electricity*, vol. 44, no. 4, pp. 411–454, 1939. [Online]. Available: http://dx.doi.org/10.1029/TE044i004p00411

[26] N. Oceanic and A. Administration, "Noaa space weather scales," http://www.swpc.noaa.gov/NOAAscales, Tech. Rep., March 2005.

[27] E. Hogan and H. Schaub, "Space weather influence on relative motion control using the touchless electrostatic tractor," in *AAS/AIAA Spaceflight Mechanics Meeting*, Santa Fe, New Mexico, Jan. 26–30 2014, Paper AAS 14-425.

[28] E. A. Hogan and H. Schaub, "Impacts of tug and debris sizes on electrostatic tractor charging performance," in *International High Power Laser Ablation and Beamed Energy Propulsion*, Santa Fe, New Mexico, April 21–25 2014.

[29] H. Schaub and Z. Sternovský, "Active space debris charging for contactless electrostatic disposal maneuvers," in *6th European Conference on Space Debris*. Darmstadt, Germany: ESOC, April 22–25 2013, paper No. 6b.O-5.

[30] S. Pfau and M. Tichy, *Low Temperature Plasma Physics: Fundamental Aspects and Applications*. Berlin: Wiley, 2001.

[31] B. T. Draine and E. E. Salpeter, "On the physics of dust grains in hot gas," *Astrophysical Journal*, vol. 231, no. 1, pp. 77–94, 1979.

[32] J. Bittencourt, *Fundamentals of Plasma Physics*. Springer-Verlag New York, Inc, 2004.

[33] L. A. Stiles, C. R. Seubert, and H. Schaub, "Effective coulomb force modeling in a space environment," in *AAS Spaceflight Mechanics Meeting*, Charleston, South Carolina, Jan. 29 – Feb. 2 2012, Paper AAS 12.

[34] S. E. DeForest, "Spacecraft charging at synchronous orbit," *Journal of Geophysical Research*, vol. 77, no. 4, pp. 651–659, 1972. [Online]. Available: http://dx.doi.org/10.1029/JA077i004p00651

[35] S. Bame, D. McComas, M. Thomsen, B. Barraclough, R. Elphic, J. Glore, J. Gosling, J. Chavez, E. Evans, and F. Wymer, "Magnetospheric plasma analyzer for spacecraft with constrained resources," *Review of scientific instruments*, vol. 64, no. 4, pp. 1026–1033, 1993.

[36] E. G. Mullen, M. S. Gussenhoven, and D. A. Hardy, "Scatha survey of high-voltage spacecraft charging in sunlight," *Journal of the Geophysical Sciences*, vol. 91, pp. 1074–1090, 1986.

[37] M. J. Mandell, I. Katz, G. W. Schnuelle, P. G. Steen, and J. C. Roche, "The decrease in effective photocurrents due to saddle points in electrostatic potentials near differentially charged spacecraft," *IEEE Transactions on Nuclear Science*, vol. 25, no. 6, pp. 1313–1317, 1978.

[38] M. J. Mandell, V. A. Davis, D. L. Cooke, A. T. Wheelock, and C. Roth, "Nascap-2k spacecraft charging code overview," *Plasma Science, IEEE Transactions on*, vol. 34, no. 5, pp. 2084–2093, 2006.

[39] S. T. Lai, "An overview of electron and ion beam effects in charging and discharging of spacecraft," *IEEE Transactions on Nuclear Science*, vol. 36, no. 6, pp. 2027–2032, 1989.

[40] D. M. Goebel and I. Katz, *Fundamentals of electric propulsion: ion and Hall thrusters*. John Wiley & Sons, 2008, vol. 1.

[41] J. R. Beattie, "Electrostatic ion thruster with improved thrust modulation," Jun. 13 1989, uS Patent 4,838,021.

[42] P. J. Wilbur, V. K. Rawlin, and J. Beattie, "Ion thruster development trends and status in the united states," *Journal of Propulsion and Power*, vol. 14, no. 5, pp. 708–715, 1998.

[43] C. Bombardelli and J. Pelaez, "Ion beam shepherd for contactless space debris removal," *AIAA Journal of Guidance, Control, and Dynamics*, vol. 34, no. 3, pp. 916–920, May–June 2011.

[44] C. Hoeber, E. A. Robertson, I. Katz, V. Davis, and D. Snyder, "Solar array augmented electrostatic discharge in geo," in *17th AIAA International Communications Satellite Systems Conference and Exhibit*, Yokohama, Japan, Feb 23-27 1998, Paper AIAA 98–1401.